Interference of p53:Twist1 interaction through competing nanobodies

Serena D'Agostino [a,1], Elisa Mazzega [b,1], Katja Praček [b,c], Sara Piccinin [a], Flavia Pivetta [a], Michela Armellin [a], Sara Fortuna [c], Roberta Maestro [a], Ario de Marco [b,*]

[a] Unit of Oncogenetics and Functional Oncogenomics, Centro di Riferimento Oncologico di Aviano (CRO Aviano) IRCCS, National Cancer Institute, Via Gallini 2, 33081 Aviano, PN, Italy
[b] Lab of Environmental and Life Sciences, University of Nova Gorica, Vipavska cesta 13, 5000 Rožna Dolina, Nova Gorica, Slovenia
[c] Department of Chemical and Pharmaceutical Sciences, University of Trieste, Via L. Giorgieri 1, 34127 Trieste, Italy

ARTICLE INFO

Keywords:
p53
Twist1
Nanobody
VHH
Intrabodies
Panning strategies

ABSTRACT

Twist1 promote the bypass of p53 response by interacting with p53 and facilitating its MDM2-mediated degradation. We reasoned that reagents able to interfere with the p53:Twist1 complex might alleviate Twist1 inhibitory effect over p53, thus representing potential therapeutic tools in p53 wild type tumors. From a pre-immune library of llama nanobodies (VHH), we isolated binders targeting the p53 C-terminal region (p53-CTD) involved in the interaction with Twist1 by using recombinant Twist1 as an epitope-specific competitor during elution. Positive hits were validated by proving their capacity to immunoprecipitate p53 and to inhibit Twist1:p53 binding *in vitro*. Molecular modeling confirmed a preferential docking of positive hits with p53-CTD. D11 VHH activity was validated in human cell models, succeeded in immunoprecipitating endogenous p53 and, similarly to Twist1 knock-down, interfered with p53 turnover, p53 phosphorylation at Serine 392 and affected cell viability. Despite the limited functional effect determined by D11 expression in target cells, our results provide the proof of principle that nanobodies ectopically expressed within a cell, have the capacity to target the assembly of the pro-tumorigenic Twist1:p53 complex. These results disclose novel tools for dissecting p53 biology and lay down the grounds for the development of innovative targeted therapeutic approaches.

1. Introduction

The p53 protein, encoded by the TP53 gene, is a transcription factor involved in the control of key biological processes including cell cycle, apoptosis, senescence, DNA repair and response to various stresses. Due to its central role in cell survival and proliferation, p53 is one of the tumor suppressors mostly involved in the control of cancer progression. In the majority of tumors the TP53 gene is mutated, yielding a dysfunctional protein. In others, *e.g.* neuroblastomas, sarcomas or leukemias, although the TP53 gene retains a wild type status, the p53 response appears attenuated, suggesting alternative inactivation mechanisms [1]. A number of p53 interacting proteins have proven to contribute to p53 functional inhibition in TP53 wild type tumors. Among these, the ubiquitin ligase MDM2 that promotes p53 proteasome-mediated degradation and is amplified in several cancers [2]. Intriguingly, a number of small molecules have been developed to target p53:MDM2 interaction and several of them are currently evaluated in clinical trials [3–5]. Such molecules have the capacity to shield p53 from MDM2 interaction and, by favoring p53 stabilization, trigger a p53-mediated tumor suppressive response (apoptosis, growth arrest, senescence).

We recently demonstrated that the basic helix-loop-helix transcription factor Twist1 binds to the C-terminal domain of p53 (p53-CTD), corresponding to residues 340–393, and modulates p53 response in TP53 wild type tumors [6]. Specifically, we showed that Twist1, by interacting with p53, facilitates its MDM2-mediated turnover, thus alleviating cells from p53 tumor suppressive activity. On these grounds, it has been suggested that the inhibition of the p53:Twist1 interaction might represent a therapeutic strategy to reactivate p53 in TP53 wild type tumors (*e.g.* sarcomas and neuroblastomas), thus unleashing a physiological tumor suppressive effect [7].

To address this hypothesis, we exploited nanobodies as a means for challenging p53:Twist1 complexes. Nanobodies, also referred to as VHH, are single chain antibodies that correspond to the variable heavy

* Corresponding author.
E-mail address: ario.demarco@ung.si (A. de Marco).
[1] These authors contributed equally to this work.

Accepted 22 November 2021

chain domain of camelid IgG2 and IgG3. They represent promising reagents because of their elevated stability and the capacity to enter also intracellular compartments (intrabody) [8]. Indeed, nanobodies have been successfully used to target intracellular antigens, including p53 [8–12]. In particular, a VHH directed against the transactivation domain of p53 has been used to translocate this protein to the mitochondrial outer membrane [13] and a nanobody targeting the DNA binding domain has been proven to hinder the interaction between p53 and papillomavirus-encoded E6AP protein, thus preventing p53 ubiquitination [12]. To the best of our knowledge, no VHH specifically targeting the p53-CTD has been reported so far, possibly due to the low antigenicity of this region.

The preferential recovery of binders specific for "difficult" epitopes can be improved by designing an *ad hoc* panning strategy. For instance, including a competitive elution step with FGF2, we were able to isolate VHHs specific for the epitope recognized by this growth factor on the receptor FGFR1 [14]. Here we sought to employ a similar competitive elution approach for the isolation of nanobodies targeting the p53-CTD region that binds toTwist1. Positive hits were then evaluated for their capacity to inhibit p53:Twist1 interaction and molecular modeling was performed to identify hypothetical contact surfaces, with the perspective to use this information for mutagenesis-based optimization.

2. Material and methods

2.1. Recombinant protein production

Human full length Twist1 (hTwist1), human full length p53 (hp53) and GFP were cloned into a Strep-Tag pPSG105. Full length p53 and a p53 fragment encompassing the CTD (aa 340–393) were cloned into a GST-tag pGEX plasmid.

These constructs, as well as empty vector plasmids, were expressed in BL21(DE3) pLysS *E. coli*. Bacteria were grown at 37 °C in LB broth until OD_{600} reached 0.6 and protein production was induced by isopropyl β-D-1-thiogalactopyranoside (IPTG) addition (1 mM for 4 h at 30 °C for Strep-tag proteins; 0.5 mM overnight at 25 °C for GST-tag proteins). Bacterial pellets were then lysed in the presence of protease inhibitors (1 mM PMSF; Complete protease inhibitor cocktail, Roche) and sonicated. For Strep-tag constructs the lysis buffer was: 100 mM Tris-HCl, pH 8, 150 mM NaCl, 1 mM EDTA. For GST-tag constructs the lysis buffer was PBS, pH 8, 1% Triton X-100, 5 mM EDTA. Recombinant proteins were purified by affinity chromatography using either Glutathione-Sepharose resin (GE Healthcare) or Strep-Tactin Sepharose Resin (IBA).

2.2. MicroScale Thermophoresis

Affinity measurements were performed in solution by MicroScale Thermophoresis (MST) using the Monolith NT.115 Pico device (Nanotemper, München). P53 was covalently labeled by NHS coupling with the fluorescent red dye NT-647 (Nanotemper, München) and used at the fixed concentration of 5.8 nM whereas the concentration of non-labeled Twist1 varied in the range 250 nM–0.007 nM. Samples in PBS containing 0.05% Tween20 were centrifuged 5 min at 11300 $\times g$ before being loaded into MST NT.115 premium glass capillaries and used for binding experiments. Data were performed in triplicate and analyzed by means of the dedicated NanoTemper software.

2.3. p53, Twist1, and VHH modeling

Sequences in FASTA format were fed to the I-TASSER server [15] without further constrains. Four possible models were obtained for both p53 and Twist. For each protein the first ranked predicted model underwent the MD protocol reported below.

The frameworks of the experimentally determined VHH sequences were searched in the protein data bank with BLAST, E-Value Cutoff 10.0 and Sequence Identity Cutoff 80%. Among the resulting sequences, those of matching length were further assessed. Sequences with the lowest number of substitutions and insertions were then chosen for homology modeling. We used the 4KSD [16] framework for the D11 VHH and 4DK3 [17] for A5, B3, C9 VHHs. Sequences were aligned and mutated with Swiss-PdbViewer 4.1 [18]. The predicted models underwent the MD protocol reported below.

2.4. MD protocol

For all the systems, we minimized the free molecules, placed the molecules in a cubic box with a water layer of 0.7 nm and Na^+ and Cl^- ions to neutralize the system, and performed a second minimization. We used AMBER99SB-ILDN [19] force field and Simple Point Charge water. We performed NVT and NPT equilibrations for 100 ps, followed by 250 ns NPT production run at 300 K. The temperature was controlled with a modified Berendsen thermostat [20], the pressure with an isotropic Parrinello-Rahman at 1 bar. The iteration time step was set to 2 fs with the Verlet integrator and LINCS [21] constraint. We used periodic boundary conditions. All the simulations and their analysis were run as implemented in the GROMACS package [22]. RMSDs have been plotted as running averages over 100 sampled points. 250 ns of MD production run (200 ns for Twist) were sampled every 25 ns. The obtained configurations were used for successive docking. Simulations were run on Marconi (CINECA, Italy). Complexes were simulated using the same protocol and their trajectories further scored with BLUUES [23].

2.5. Docking

We used the web interface of HADDOCK [24] with its standard parameters. System dependent active residues were defined for each VHH as their CDR, while for p53 and twist we used both the experimentally determined domain identified in Piccinin et al. [6] and CPORT predicted interface [25], while passive residues were automatically defined in all cases. The parameters set were then fed both to the "easy" interface and the "prediction" interface of HADDOCK. Among the docking results obtained, we chose the docking cluster with the lowest score. The predicted models underwent the MD protocol reported above.

2.6. Library panning and VHH isolation

VHH library was generated by cloning into the pHEN4 vector the PCR products of the cDNA of non-immunized llama lymphocytes using primer primers annealing to the common CH2 exon of the heavy chain llama immunoglobulins and to the leader sequence. Panning procedures were as previously detailed [26]. Epoxy magnetic beads (Invitrogen) were first washed in PBS using a magnetic trap to separate them from the supernatant and finally resuspended in 1 ml of the same buffer. An aliquot of 50 µl was then incubated with 100 µg of full-length p53-strep tag (target antigen) whereas 100 µl were incubated with 200 µg of GFP-strep tag to use as the depletion material. Both bead aliquots were incubated overnight at 4 °C under constant rotation, washed 3 times in PBS and resuspended in 1 ml of blocking solution (2% milk and 0.1% Tween20 in PBS). In parallel, 10^{11} phages from the pre-immune library were resuspended in 1 ml of blocking solution and incubated 30 min at 21 °C under constant rotation. The depletion beads were recovered and split in two aliquots. The first aliquot was incubated 1 h at 21 °C with the saturated phage sample. The beads were discharged and the supernatant was then incubated with the second depletion sample. The finally recovered phage supernatant was added to the beads coated with p53 and incubated 2 h at 21 °C under constant rotation. The beads were then recovered using the magnetic support, the supernatant was removed and 10 ml of PBS + 1% milk were added and used to wash the beads. After ten washing cycles, phages were first eluted by competition by adding 100 nmol of Twist1 and incubating the samples 30 min at room temperature. The remaining bound phages were eluted by rocking the beads

for 10 min at room temperature in 0.9 ml of 0.2 M glycine-HCl, pH 2.2, BSA 1 mg/ml. The elution fraction was then neutralized with 250 µl of borate buffer, pH 9.1, and glycerol was added to reach 10%. The elution fractions (competitive and non-competitive) were stored at −80 °C, apart 750 µl that were used to infect 9.25 ml of TG1 cells (OD_{600} nm = 0.5). The cells were grown 30 min at 37 °C, then pelleted and resuspended in 1.8 ml of 2xTY medium. Finally, bacteria were spread on large 2xTY-1% glucose + ampicillin plates (600 µl/dish) and grown overnight at 30 °C. Grown bacteria were recovered and mixed with helper phages for amplifying the clones isolated by the first panning round. Phages were then precipitated on ice by adding PEG (30% w/v), pelleted (1800 ×*g* at 4 °C for 10 min) and finally resuspended in PBS, 10% glycerol, before being used for a second panning round. The screening of the clones recovered after the second panning was performed by ELISA using the supernatant fractions of the bacterial culture and 200 ng/well of GFP-strep tag as the negative control and p53-strep tag as the positive control. Putative positive clones were validated by repeating the ELISA in triplicate and finally sequenced to identify unique sequences.

2.7. VHH production

VHH sequences were subcloned into a modified pET-14b vector to produce recombinant GFP- or Fc-6xHis-fusion proteins [27,28] in *E. coli* BL21 (DE3) cells co-expressing DsbC and sulfhydryl oxidase and grown in LB media, shaking at 220 rpm and temperature at 37 °C. The temperature was lowered to 20 °C when the OD_{600} reached the value of 0.4 and arabinose was added at the concentration of 5 mg/ml. IPTG (0.2 mM) was provided after 30 min and bacteria were grown overnight before being pelleted and then resuspended in four volumes of lysis buffer (50 mM TrisHCl, pH 8, 500 mM NaCl, 10 mM imidazole, 0.25 mg/ml lysozyme, 50 µg/ml DNAse, 5 mM $MgCl_2$. Lysis was facilitated by sonication on ice, the supernatant was recovered after centrifugation (30 min at 30000 ×*g*) and then loaded on a 1 ml Hi-Trap NiNTA column (Qiagen). After washing, Fc- and GFP-VHHs were eluted in 50 mM TrisHCl, pH 8, 500 mM NaCl, 300 mM imidazole and buffer exchanged into 30 mM HEPES, pH 7.2, 100 mM NaCl, 1 mM DTT, 20% glycerol.

Intrabodies were obtained applying the same protocol to VHHs expressed in wild type BL21 (DE3).

2.8. Immunoprecipitation, epitope-specificity and competition assays

Pull-down experiments were performed by incubating overnight 25 µl of epoxy magnetic beads (Dynabeads, ThermoFisher) with 5 µg of purified GFP-VHHs in PBS pH 7.4 plus 2 mM EDTA. Beads incubated with 5 µg of a mouse monoclonal anti-p53 antibody were used as a positive control. Beads incubated with BSA or an irrelevant VHH [27] were used as a negative control (CTR). After 3 washing steps in PBS, GST-p53 (10 µg) was added to all samples and incubated for 2 h. After 3 washing steps, beads were resuspended in SDS loading buffer. The bound proteins were separated by SDS-PAGE, blotted on nitrocellulose membrane and probed with anti-GFP (9F9.F9, AbCam) and anti-p53 antibodies (DO1, Santa Cruz) to identify VHHs and p53. Anti-mouse secondary antibodies were ab6728 (AbCam). The same procedure was performed to identify the binding of the nanobodies to the C-terminal (aa 356–393) domain of p53 (p53-CTD). Since p53-CTD was fused to GST, VHHs and p53-CTD were identified by anti-GFP (9F9.F9, AbCam) and anti-GST (3G10/1B3, AbCam) antibodies, respectively. As a further control, 25 µl of glutathione agarose beads (Thermo Scientific) activated with 5 µg of recombinant GST were used to pull-down 10 µg of each of the GFP-VHHs. Both anti-GFP and anti-GST (3G10/1B3, AbCam) were used to identify VHHs and GST, respectively.

The competition effect of VHHs on the binding between Twist1 and p53-CTD-GST was assayed essentially as in Piccinin et al., [6]. Briefly, GST-tagged recombinant p53-CTD (5 µg) was bound to glutathione agarose beads (Thermo Scientific) and then incubated 2 h in the presence of STREP-tagged recombinant Twist1 (15 µg). To assess the capacity of VHH to compete with Twist1 for p53-CTD binding, each VHH (15 µg) was individually added to the p53:Twist1 mix and incubated for 1 h. Finally, GST (p53) pull-down, SDS-PAGE separation and blotting were performed as previously described [6]. Anti-Twist1 (2C1a, Santa Cruz), anti-GST (3G10/1B3, AbCam) and anti-GFP (9F9.F9, AbCam) antibodies were used to identify the target proteins. A reaction with GST-only was performed in parallel as a negative control.

VHH epitope binning was performed by competitive binding to p53 essentially as above with the following modifications. STREP-tag full length p53 (10 µg), previously bound to Streptavidin coated magnetic beads (Dynabeads, ThermoFisher), was incubated with a D11 VHH (10 µg) expressed as a fusion protein with the human Fc domain. After several washings, 10 µg of each GFP-fused VHH were individually added to the mix. After p53 pull down, co-precipitated proteins were analyzed by SDS-PAGE. Anti-GFP (9F9.F9, AbCam) was used to detect the VHH that were capable of competing with D11 for p53 binding. The DO1 (Santa Cruz) antibody was used for p53 visualization. All results were confirmed on at least three independent experiments.

2.9. VHH expression in human cell lines and co-immunoprecipitation experiments

To generate mammalian expression vectors, the sequences of D11 and of an irrelevant VHH (Cy1) directed against a *Cyanobacteria* epitope [29] were subcloned from pET vectors into pCS2 vector to obtain pCS2-myc-VHHs, with or without an ectopic nuclear localization signal (pCS2-myc-NLS). Finally, myc-NLS-D11 and myc-NLS-Cy1 were subcloned into the pLVX-IRES-ZsGreen1 (pLIZ) lentiviral vector.

HEK293T and HT1080 human cell lines (ATCC) were maintained at 5% CO_2 in Dulbecco's Modified Eagle's medium (DMEM, Life-Technologies) supplemented with 10% heat-inactivated fetal bovine serum (Life-Technologies) and were transfected as previously described [6]. For lentiviral production, HEK293T were co-transfected with PMD2.G, psPAX2 together with myc-tag-D11, myc-tag-Cy1 VHH or pLIZ empty vector. Culture supernatants were harvested 48 hour post transfection and used to infect HT1080. Infected cells were selected by fluorescence-activated cell sorting (FACS) on the basis of ZsGreen positivity. VHH-infected cells were compared to short hairpin silenced Twist1 (shTwist1)-infected HT1080 [6] to assess the effect of abrogation of Twist1:p53 interaction on p53.

Immunofluorescence was essentially as described before [30]. Briefly, HT1080 cells engineered with pLIZ lentiviral vectors to express myc-tagged VHH were cultured on coverslips. After fixation (4% paraformaldehyde/PBS, 10 min at room temperature), cells were permeabilized (0.25% TritonX-100 in 0.1% BSA/PBS, 10 min) and incubated in blocking buffer (0.05% TritonX-100 in 3% BSA/PBS, 30 min). After repeated washings with PBS, slides were stained with an anti-myc antibody (9E10, Santa Cruz) at 4 °C overnight. Primary antibodies were visualized with goat anti-mouse Alexa Fluor 594 (Thermo Fisher Scientific). Nuclei were counterstained with DAPI. Images were recorded with a Nikon Eclipse-Ti fluorescence microscope.

Co-immunoprecipitation (Co-IP) assays were performed to assess whether nanobodies bound endogenous wild-type p53. To this end, HEK293T cells were transfected with either pCS2-myc-NLS-D11 or pCS2-myc-NLS-Cy1. pCDNA3-myc-GFP and pCS3-myc-mouse Twist1 were used as negative and positive control, respectively. Forty eight hours post-transfection cells were harvested and processed as previously described [6]. Anti-p53 (DO1, Santa Cruz) was used for immunoprecipitation. Immunoprecipitates were separated by SDS-PAGE and transferred onto nitrocellulose membranes (Protran, Merck). After 1 hour blocking in 5% milk in TBST (Tris-Buffered Saline Tween-20), membranes were incubated overnight at 4 °C with either anti-myc (9E10, Santa Cruz) or anti-p53 (DO1) primary antibodies. Immunoreactivity was detected with appropriate HRP-labeled secondary antibodies (Perkin Elmer) and Western Lightning Chemiluminescence Reagent Plus (Perkin Elmer).

For standard immunoblot analysis, cells were scraped from plates and lysed in RIPA buffer (Santa Cruz Biotechnology) supplemented with complete protease inhibitor cocktail (Roche Diagnostics) and 1× Pefabloc SC (Sigma). After SDS-PAGE, membranes were incubated overnight at 4 °C with the primary antibody: anti-p53 (DO1, Santa Cruz), anti-phospho S392-p53 (ab59207, AbCam), anti-Twist1 (Twist2C1a, Santa Cruz) or anti-myc (9E10, Santa Cruz). Anti-GAPDH (6C5, Santa Cruz) was used for protein loading normalization.

The chemidoc XRS+ system (Bio-Rad) and ImageLab imaging software (Bio-Rad) were used to record and analyze images, respectively. All results were confirmed on at least three independent experiments.

2.10. Cell viability assay

HT1080 cells, engineered with pLIZ lentiviral vectors to express D11 or Cy1 nanobodies, were seeded in 96-well plates (5–10 × 10^3 cells/well). The following day, after PBS washing, serum-supplemented (control) or serum-free medium (serum starvation) was added to the cultures. After 24 or 48 h, cells were fixed in 7% trichloroacetic acid (TCA) overnight at 4 °C and then extensively washed in distilled water. After drying, cell plates were stained with 0.4% (w/v) sulforhodamine B (SRB) in 1% acetic acid (30 min), then washed with 1% glacial acetic acid to eliminate the unbound dye. The bound SRB was solubilized by adding 100 µl/well of 10 mM of unbuffered Tris base solution (10 min on shaker). The optical density of each well was determined at 550 nm by using an InfiniteM1000 PRO miniplate reader (TECAN Group LTD, Mannedorf, CH). The relative cell viability was calculated using the following formula: [(A_{550} of serum starved sample / A_{550} of control sample) × 100]. Three independent experiments done in sextuplicate were statistically evaluated by using the *t*-test.

3. Results and discussion

As a first step towards the generation of Twist1:p53 competing VHH, we measured the p53:Twist1 affinity in solution. Bacterially produced recombinant full length Strep-Twist 1 and GST-p53 proteins were used in thermophoresis assays to determine the stability of the binding under physiological conditions. As reported in Fig. 1a, the apparent binding affinity of Twist1 for p53 was surprisingly high (K_D = 2.1E^{-9} M) in comparison to that measured by Noguchi and coll. for MDM2 or MDMX (0.8E^{-6} and 2.2E^{-6} M, respectively, [31]). Noteworthy, in that work the affinity was measured by fluxing soluble analytes over immobilized ligands [31], whereas we evaluated the interaction with both species in solution. Moreover, different from Noguchi and coworkers, who used monomeric peptides, we used full-length proteins, and both p53 and Twist1 can form homopolymers (tetramers and dimers, respectively) [32,33]. Thus, avidity could significantly contribute to the strength of the interaction observed in our experimental conditions.

As a second step, to gain information about the surfaces involved in the interaction and their binding strength, we modeled the Twist:p53 complex. Compared with our previous study [6], here we adopted a modeling strategy that takes into consideration multiple conformations for both binding partners. The models, built by iterative threading [15], underwent 250 ns molecular dynamics (MD) simulation to determine the individual thermodynamic stability of both p53 and Twist1 and their possible structural configurations. The root mean square deviation (RMSD), that measures how much a protein configuration deviates from its initial conformation, and its cluster analysis revealed that the p53 trajectory relaxes to a first equilibrium configuration after 25 ns and to a novel configuration at 200 ns (Suppl. Fig. 1a, left). The latter configuration is less packed than the former, as shown by the radius of gyration (Rg). This results from the opening of the helical region of the protein, as indicated by spikes in the root mean square fluctuation (RMSF) (Insets in Suppl. Fig. 1b, left). p53 closed and open configurations resulting from cluster analysis were then considered for subsequent dockings. The Twist1 structure obtained by homology modeling is elongated and

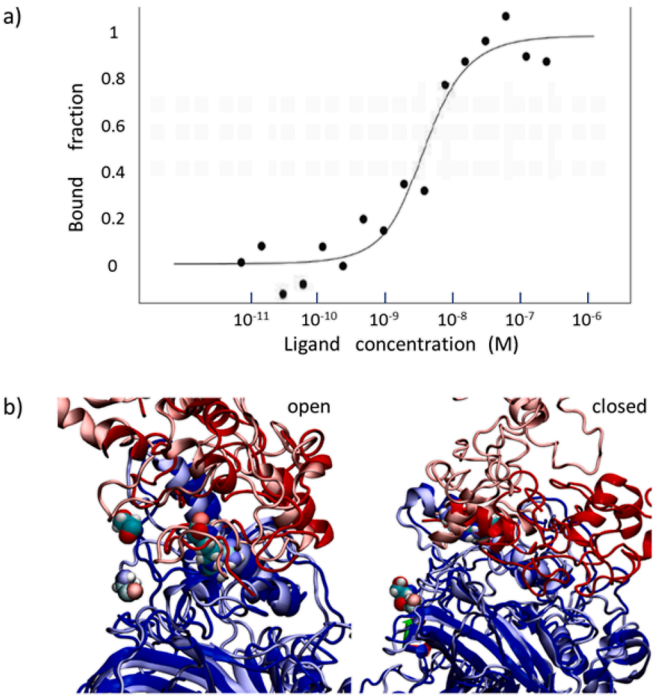

Fig. 1. p53:Twist1 interaction.
a) Thermophoresis experimental data relative to the p53/Twist1 interaction in solution. b) Detail of p53/Twist1 interaction, with p53 in open and closed configuration. The cartoon represents p53 (blue) and Twist (red) at time 0 (light colors) and after 110 ns of MD simulation (dark colors). Van der Waals spheres (oxygen red, carbon cyan, nitrogen blue, hydrogen white) are shown for p53 residues Ser392 and Arg191. Initial (light color) and final (dark colors) Arg191 configurations overlap, while Ser392 moves towards Twist1. (For interpretation of the references to color in this figure legend, the reader is referred to the web version of this article.)

mainly composed by helices. Along the MD simulation, its structure changed conformation over 50 ns, as observed by following its RMSD. Then it settled to a collapsed conformation, a change indicated by its Rg which falls and converges to the value of 2 nm (Suppl. Fig. 1a, right). Here the structure remains highly flexible when compared to p53, as indicated by higher RMSF values (Suppl. Fig. 1b, right). As the protein is highly flexible throughout the whole trajectory, Twist1 configurations were sampled every 25 ns for subsequent docking.

High Ambiguity Driven protein−protein Docking (HADDOCK) [24] was used to identify all possible p53:Twist1 complexes. Both the binding interface predicted by CPORT [25], corresponding to full length p53 solvent-exposed residues, as well as the p53-CTD were considered. This analysis took into consideration multiple conformations for both binding partners. Specifically, higher binding possibility (highest negative scores) for both open and closed p53 conformation were obtained for the complex formed by Twist1 and p53-CTD, namely the C-terminal Twist box region (Table 1, p53 open: full length −78.5 *vs* CTD 115.6; p53 closed full length −106.3 *vs* CTD -114.9). CPORT predicted also an alternative binding site for Twist1 involving the N-terminus of p53 in closed conformation through an epitope formed by the residues 43–49, 89–93, 171–181, and 241–248 (Suppl. Fig. 2a). The previously indicated interaction through direct H-bond between the Arg191 of Twist1 and the Ser392 of p53 [6] was not evident at the initial moment of the MD simulation since Arg191 appeared buried in all the predicted complexes. However, along the time Ser392 moved towards Arg191 burying itself in Twist1 and becoming inaccessible to the solvent in both open and close p53 configurations (Fig. 1b). It is interesting to note that the same Twist1 region around Arg191 (WR or Twist box domain) responsible for p53 binding is apparently involved in the binding of Twist1 to other transcription factors including RUNXs [34], SOX9 [35] and RELA

Table 1
Docking scores for the complexes formed between p53, either full length or p53-CTD, and the isolated VHHs (D11, A5, B3, C9). Docking scores for Twist1 are shown as a reference. Each score is averaged over the most favorable cluster identified by HADDOCK. The number of configurations of each cluster is shown between brackets.

Binder	p53 open		p53 closed	
	Full length	p53-CTD	Full length	p53-CTD
D11	−75.2 ± 4.8 (6)	−79.6 ± 3.7 (9)	−79.4 ± 10.9 (11)	−64.7 ± 5.9 (166)
A5	−101.0 ± 4.3 (57)	−100.1 ± 20.8 (6)	−87.2 ± 4.4 (19)	−73.8 ± 3.7 (57)
B3	−66.3 ± 6.6 (13)	−72.1 ± 6.5 (9)	−64.6 ± 18.7 (4)	−91.7 ± 8.4 (12)
C9	−52.2 ± 18.2 (4)	−69.0 ± 9.1 (4)	−87.9 ± 24.3 (15)	−75.7 ± 3.6 (31)
Twist1	−78.5 ± 6.3 (391)	−115.6 ± 7.5 (112)	−106.3 ± 14.1 (15)	−114.9 ± 9.4 (43)

[36,37].

The analysis essentially substantiated our previous results [6] obtained with a different docking strategy that indicated p53-CTD as the major epitope bound by Twist1. Next we set out to identify competitor nanobodies capable of specifically interfering with this interaction. *In vitro* panning of pre-immune phage display libraries is a very flexible technology to isolate binders for potentially any antigen and with specific biophysical features [14,38,39]. We therefore designed a protocol to recover VHH specific for p53-CTD with the long-term purpose to use them *in vivo* for preventing the p53:Twist1 interaction. The library was first depleted against GST and the unbound fraction challenged with GST-p53 (full length). Competitive elution of the bound phages was performed by adding a molar excess of Strep-Twist1. Four different clones (A5, B3, C9, D11) were selected after panning, screening and sequencing (Suppl. Fig. 3 and Suppl. Table 1).

The selected VHHs were sub-cloned to be produced as GFP-fusion reagents and tested in pull-down experiments for their capacity to immune-purify GST-p53 from a solution. All four VHH succeeded in capturing full-length p53 as efficiently as a p53-specific mouse monoclonal antibody directed against the N-terminus of p53 (DO1) (Fig. 2a). When the VHH were probed against recombinant p53-CTD, two VHH, A5 and in particular D11, demonstrated higher recovery capacity (Fig. 2b). Despite the apparent variable binding capacity, all VHH seemed to be able to compete with Twist1 for p53-CTD binding since the formation of the p53:Twist1 complex was inhibited by the addition of any of the GFP-VHH (Fig. 3). Moreover, competitive pull-down, performed to assess whether the different VHHs recognized a (partially) overlapping epitope on p53-CTD, indicated that in the presence of D11 the capture of p53 by A5 and C9 was somehow prevented, suggesting steric hindrance (Suppl. Fig. 4).

Next we tried to model the molecular mechanisms by which the VHHs interfered with the p53:Twist1 interaction. To this aim, the VHH built by homology modeling followed by 250 ns MD was docked to the corresponding interfaces of p53 in both closed and open conformations. The HADDOCK scores, especially those for p53 open conformation, confirmed the suitability of VHH to bind to p53-CTD (Table 1), in line with *in vitro* pull-down results (Fig. 2). The simulations showed a clear steric overlap between Twist1 and the two clones with highest p53-CTD binding capacity, namely A5 and D11 (Fig. 4 and Suppl. Fig. 5). MD simulations revealed that the A5:p53 and D11:p53 complexes do not change their backbone, as their RMSD did not exceed 0.2 nm. This despite the fact that VHH are highly mobile on their binding sites, as indicated by their backbone RMSD with respect to the backbone of the target p53 as high as 1.5 nm (Suppl. Fig. 6). Interestingly, A5 and Twist1 were predicted by CPORT to share also the alternative N-term epitope on p53 discussed above (Suppl. Fig. 2b–c).

The nature of the binding can be assessed by counting the number of

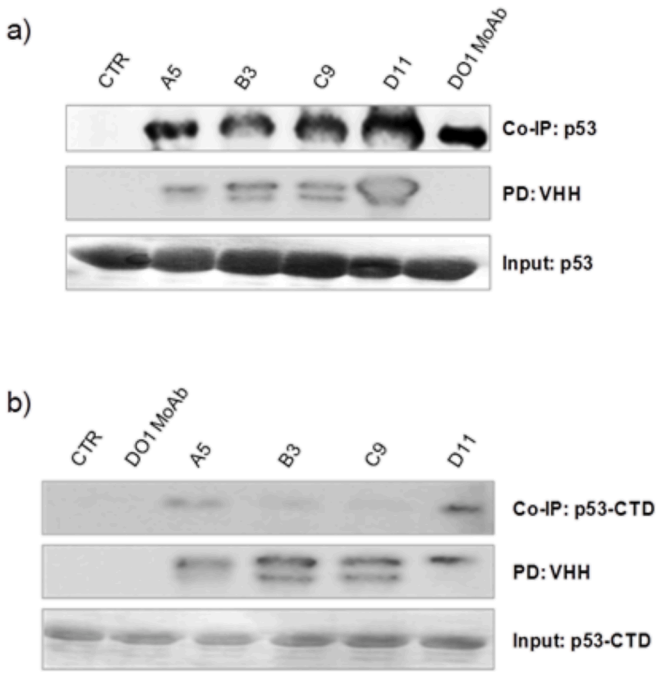

Fig. 2. Selected VHHs specifically immunocapture p53.
The indicated GFP-tagged VHHs (A5, B3, C9, D11), previously immobilized on magnetic beads, were incubated with either GST-tagged p53 full length (a) or p53-CTD (b) and used as preys in pull-down experiments. For positive and negative control (CTR), beads functionalized with a mouse monoclonal anti-p53 antibody (DO1 MoAb) or with BSA were used instead of VHH. VHH (preys) were detected with anti-GFP antibodies. Co-immunopurified (Co-IP) p53 and p53-CTD were detected with an anti-p53 monoclonal antibody (DO1 MoAb).

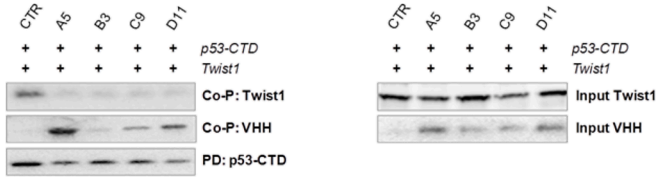

Fig. 3. VHH directed against p53-CTD compete with Twist1 for p53 binding.
Recombinant GST-tagged p53-CTD was incubated with STREP-tagged Twist1. After incubation, the indicated VHH were individually added to the mix. No VHH was added to the control reaction (CTR). GST pull down (PD) for p53-CTD resulted in co-pull down (Co—P) of VHH and Twist1 (left panel). The amount of co-purified Twist1 was significantly reduced in the presence of VHH. Twist1 and VHH inputs are reported in the right panel.

contacts and hydrogen bonds between each VHH paratope, formed mainly by the complementarity determining regions (CDR), and p53 (Fig. 5). Qualitatively, all CDRs in A5 contributed to the paratope, which was instead mostly limited to CDR3 in D11. This may be due to the different CDR3 length in the two VHH (18 residues in D11, 9 in A5) and their consequent alternative conformation arrangement. When p53 was in the open configuration, the CDR3 of A5 contributed mostly, with up to 1500 contacts, while CDR1 contacts were limited to 250. For the same configuration, in the first 100 ns D11 bound p53 mainly thanks to its CDR1, whereas later CDR3 built the majority of the contacts with the antigen and CDR2 never contributed to the binding. When p53 was in its closed conformation, all CDRs of A5 participated, while D11 CDR3 contributed with up to 2000 contacts. Both A5 and D11 formed up to 12 hydrogen bonds. Each A5 CDR contributed with up to 4 hydrogen bonds in all the explored complexes, while the CDR3 of D11 participated with up to 3 (p53 open) and 6 (p53 closed) hydrogen bonds (Fig. 5).

Both the *in silico* and biochemical results converged to the conclusion

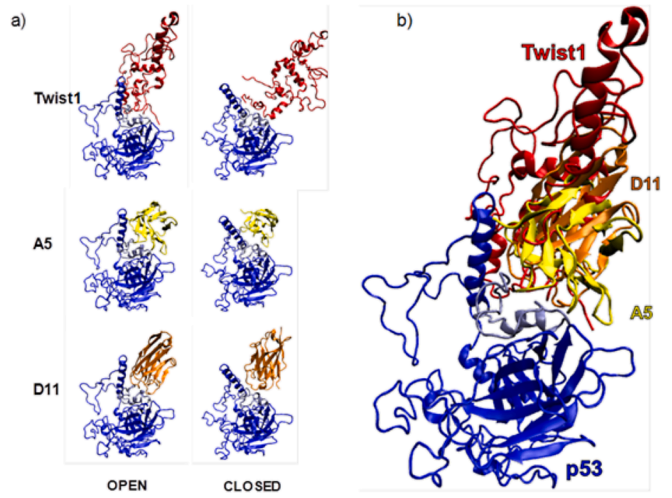

Fig. 4. End-simulation configurations of the VHHs/p53 complexes.
a) Snapshots at 250 ns of Twist1 (red), A5 (yellow) and D11 (orange) on p53 (blue; light blue, docking site) in open and closed configurations. b) Overlap of the open configurations. (For interpretation of the references to color in this figure legend, the reader is referred to the web version of this article.)

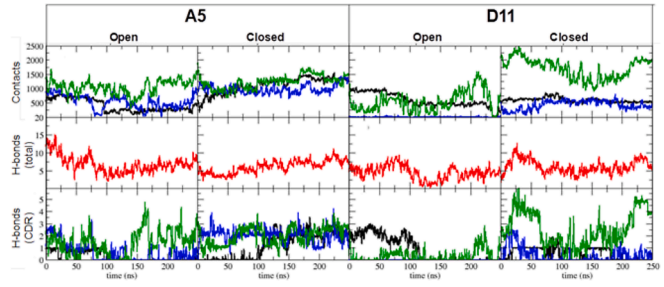

Fig. 5. Modeling of the molecular interactions established by p53 with A5 and D11 VHH.
The upper panels report the number of contacts at a distance <0.6 nm, established by p53 with each CDR of A5 and D11, as a function of time, p53 is represented in closed and open configuration. Color code: CDR1, black; CDR2, blue; CDR3, green. The red line indicates the total number of hydrogen bonds (H-bonds total) established by the p53 protein with A5 and D11. The lower panels report the number of hydrogen bonds between p53 and each CDR of A5 and D11. Running averages over 50 datapoints are reported. (For interpretation of the references to color in this figure legend, the reader is referred to the web version of this article.)

that we successfully selected some VHH specific for the CTD region of p53 bound by Twist1. This achievement demonstrated the effectiveness of our panning strategy to selectively isolate binders for epitopes that are scarcely immunogenic. Nanobodies directed against such "difficult" epitopes would be usually lost in standard selection conditions because disadvantaged with respect to antibodies binding to epitopes that are better structured and therefore offer stronger interaction surfaces. In our approach we forced the *in vitro* selection towards an acceptable compromise: the isolation of VHHs specific for a predetermined epitope even at the cost of below-average biophysical characteristics. In particular, only D11 could be produced effectively as a soluble immunoreagent under both oxidizing and reducing conditions (Suppl. Table 1), namely it was the optimal candidate not only for folding correctly in oxidative cell compartments (prokaryotic periplasm and eukaryotic ER/Golgi) but also as an intrabody in the reducing conditions of cellular cytosol. This was confirmed by the immunofluorescence experiments. D11 displayed a diffuse nucleocytoplasmic staining pattern when expressed in mammalian cells (Suppl. Fig. 7), confirming its characteristics of soluble and monodispersed intrabody. Thus, D11 was selected for further validation experiments. To address its capacity to biologically interfere with a nuclear protein such as p53, the sequences of D11 and of an irrelevant VHH (Cy1) directed against cyanobacteria proteins were subcloned in frame with an N-terminus nuclear localization signal (NLS) to drive them into the nucleus. The resulting constructs were expressed in p53 wild type cell lines (HT1080 and HEK293T). Immunofluorescence confirmed a predominant nuclear accumulation with a diffuse and uniform staining (Suppl. Fig. 7). Immunoprecipitation of p53 in HEK293T cells transfected with myc-tagged constructs indicated that D11 bound endogenous p53 as efficiently as Twist1 (Fig. 6a). We then assessed the biological effect of D11 delivery. Similar to Twist1 silencing (shTwist1) in HT1080 cells, multiple independent experiments indicted that the ectopic expression of D11 induced a slight but reproducible increase (20–30%) in the levels of the endogenous p53 protein (Fig. 6b and Suppl. Fig. 8a), when compared to both Cy1 VHH engineered cells and empty vector infected cells (CTR). Furthermore, similar to what previously reported for Twist1 silencing [6] (Suppl. Fig. 8b), D11 expression correlated with an augment of the fraction of p53 phosphorylated at Serine 392 (S392) (Fig. 6c), a residue that is involved in the control of p53 stability and functions [40]. Of course, quantitatively higher p53 increases would enable more reliable measures of the biological effects of the D11 ectopic expression. Nevertheless, we observed that under stress conditions (serum starvation) cell viability was reduced in D11 engineered cells (Fig. 6d), once again similar to what observed after Twist1 knock down [6]. Although not reaching statistical significance ($p = 0.20$ and $p = 0.29$ at 24 and 48 h, respectively), the trend was confirmed in multiple independent repeats. Overall, the finding that D11 delivery mimics the previously reported biological effects of Twist1 silencing in the same cell model [6] supports the notion that the

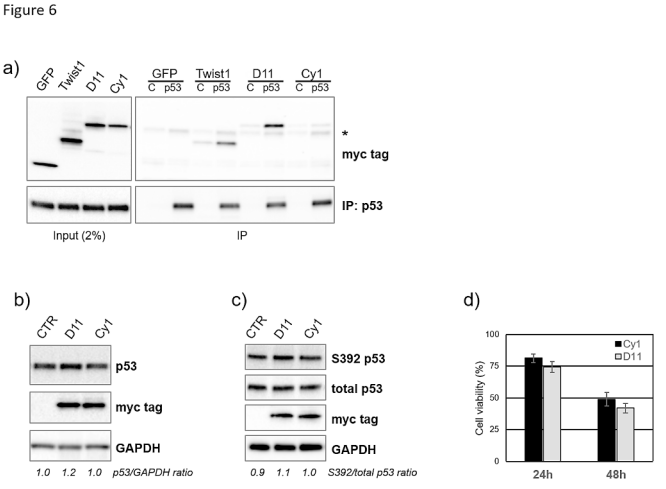

Fig. 6. D11 binds to endogenous p53 and mimics the effect of Twist1 silencing on p53.
a) D11 binds to endogenous p53. Endogenous p53 was immunoprecipitated (IP) from cells engineered with myc-tagged GFP, Twist1, D11 or an irrelevant VHH (Cy1). Immunoprecipitation with pre-immune IgG2A antibodies was carried out in parallel as a control (C). Co-precipitated proteins were detected with anti-myc antibodies. The asterisk indicates the antibody heavy chains.
b) Total p53 and c) S392-phosphorylated p53 levels increase in D11 expressing cells. Protein lysates from HT1080 cells engineered to stably express myc-tagged D11, an irrelevant VHH (Cy1) or the empty lentiviral vector (CTR) were separated by SDS-PAGE and probed with the indicated antibodies. GAPDH was used for protein normalization. p53/GAPDH and S392 p53/total p53 signal ratios are indicated.
d) D11 affects cell viability under serum starvation. HT1080 cells engineered to express D11 were serum starved for 24 or 48 h and cell viability was assessed by SRB assay. After serum starvation, viability of D11 engineered cells, which express higher p53 levels (b), was tendentially reduced compared to Cy1 control cells (data confirmed in four independent experiments). Error bars indicate mean ± SEM.

nanobody competes with Twist1 for p53 binding also within a cell. This discloses the possibility of using nanobody-based approaches to reactivate p53 in those tumors that retain a wild type TP53 gene but rely on alternative mechanisms, such as Twist1 overexpression, to inhibit the p53 response, such as sarcomas and neuroblastomas [6,7].

4. Conclusions

In this work we provided the proof of principle that nanobodies targeting the unstructured C-terminal region of p53 can be efficiently isolated by combining the screening of a pre-immune library with a panning strategy aimed at identifying, among the different binders, only those binding to such epitope. Specifically, we isolated VHHs targeting the p53-CTD by competitive elution with Twist1, known to bind to this domain. The method is suitable to isolate selectively reagents that have the potential to interfere with only one function of hub proteins. Despite the fact that they can have worse binding affinities than binders specific for other antigen epitopes, they can still prevent substantially and specifically the targeted function [14]. The recovered VHH displayed intrabody features and were able to interact with p53, both in biochemical assays and within a cell, as well as to affect p53 interaction with Twist1, indicating that nanobodies may be adopted to tune biological phenomena regulated by reversible protein complexes. In this perspective, they might become precious reagents for elucidating molecular mechanism independently on their therapeutic suitability. In our case, one selected VHH (D11) mimicked the effect of Twist1 silencing in terms of relief of p53 turnover, p53 phosphorylation at Serine 392 and sensitivity to stress conditions, corroborating the notion of the potential use of such reagents as a mean to antagonize Twist1:p53 interplay in tumors. Importantly, p53-CTD, which is target of extensive post-translational modifications and protein-protein interactions, plays a key role in regulating p53 tumor suppressive functions and is required for optimal MDM2-mediated degradation [41]. Thus, D11 might reveal an important tool to interfere in a wider manner with p53 biological activities. Of course, D11 is to be considered a hit molecule that needs further improvements to impact more substantially on p53 biological readouts. The modeling data collected in this work are functional to this development since provide detailed structural information about the modality of interaction between VHH, p53 and Twist1, thus paving the ground for second generation VHH, optimized for their binding/inhibitory characteristics. The power of our combined method, which integrates the rapid panning allowed by pre-immune libraries with *in silico* clone optimization, has been recently confirmed by other groups [42,43] that underlined its flexibility and effectiveness also for the isolation of mutation-specific nanobodies.

Therapeutic applications based on circulating nanobodies present a number of limitations, among which the short half-life in biological fluids and the fast renal clearance. Nevertheless, the promising advantages of nanobody-based technology (*e.g.* strong antigen-binding affinity, low intrinsic immunogenicity [44], simple engineering and scalable dimension, hydro solubility) have prompted a large number of clinical trials (over 40 trials registered in the https://clinicaltrials.gov database for nanobodies and nanobody-based constructs such as bivalent, bispecific or derivatized molecules) and recently both the US Food and Drug Administration (FDA) and the European Medicines Agency (EMA) have approved the first nanobody (caplacizumab) for treatment of a blood clotting disorder [45]. Nanobody-based intrabodies, in contrast, have not yet proposed for clinical applications but it is tempting to speculate that the mRNA technology, successfully used for anti-COVID19 vaccination [46], might be employed for further improving intracellular transfer of interfering nanobody-intrabodies with therapeutic potential.

CRediT authorship contribution statement

RM and AdM conceived the work, EM isolated, produced and characterized the nanobodies, SDA, SP, FP, and MA performed the experiments with mammalian cells and prepared the recombinant proteins, KP and SF performed the *in silico* simulations, SF, RM and AdM wrote the draft and all the authors checked and approved it.

Declaration of competing interest

The authors declare that they have no known competing financial interests or personal relationships that could have appeared to influence the work reported in this paper.

Acknowledgments

The authors wish to thank Marek Zurawski (NanoTemper Technology) for technical support. This study was supported by: “TALENTS3 program” (European Social Fund 2014/2020 Regional Operative Programme, Axis 3 – Education and Training Call n. 782 of 13/04/2015) to SF; the Italian Association for Cancer Research (AIRC), (AIRC-IG grant to RM); Ministero della Salute-Ricerca Finalizzata (to RM). The research leading to these results has received funding from AIRC under IG 2020 - ID. 24589 project – P.I. Sara Fortuna. We acknowledge the CINECA (including Awards N. HP10CG7JPW, 2017 and N. HP10BTJPER, 2017) for the availability of high performance computing resources and support.

Appendix A. Supplementary data

Supplementary data to this article can be found online at https://doi.org/10.1016/j.ijbiomac.2021.11.160.

References

[1] E.R. Kastenhuber, S.W. Lowe, Putting p53 in context, Cell 170 (2017) 1062–1078, https://doi.org/10.1016/j.cell.2017.08.028.
[2] J.D. Oliner, A.Y. Saiki, S. Caenepeel, The role of MDM2 amplification and overexpression in tumorigenesis, Cold Spring Harb. Perspect. Med. 6 (2016), a026336, https://doi.org/10.1101/cshperspect.a026336.
[3] G. Sanz, M. Singh, S. Peuget, G. Selivanova, Inhibition of p53 inhibitors: progress, challenges and perspectives, J. Mol. Cell Biol. 11 (2019) 586–599, https://doi.org/10.1093/jmcb/mjz075.
[4] J.L. Silva, C.G.S. Lima, L.P. Rangel, G.D.S. Ferretti, F.P. Pauli, R.C.B. Ribeiro, T. B. da Silva, F.C. da Silva, V.F. Ferreira, Recent synthetic approaches towards small molecule reactivators of p53, Biomolecules 10 (2020) 635, https://doi.org/10.3390/biom10040635.
[5] M.J. Duffy, N.C. Synnott, S. O'Grady, J. Crown, Drugging "undruggable" genes for cancer treatment: are we making progress? Int. J. Cancer 148 (2021) 8–17, https://doi.org/10.1016/j.semcancer.2020.07.005.
[6] S. Piccinin, E. Tonin, S. Sessa, S. Demontis, S. Rossi, L. Pecciarini, L. Zanatta, F. Pivetta, A. Grizzo, M. Sonego, C. Rosano, A.Paolo Dei Tos, C. Doglioni, R. Maestro, A “twist box” code of p53 inactivation: twist box: p53 interaction promotes p53 degradation, Cancer Cell 22 (2012) 404–415, https://doi.org/10.1016/j.ccr.2012.08.003.
[7] T.R. Hupp, R.L. Hayward, B. Vojtesek, Strategies for p53 reactivation in human sarcoma, Cancer Cell 22 (2012) 283–285, https://doi.org/10.1016/j.ccr.2012.08.020.
[8] E. Soetens, M. Ballegeer, X. Saelens, An inside job: applications of intracellular single domain antibodies, Biomolecules 10 (2020) 1663, https://doi.org/10.3390/biom10121663.
[9] M. Summanen, N. Granqvist, R.K. Tuominen, M. Yliperttula, C.T. Verrips, J. Boonstra, C. Blanchetot, E. Ekokoski, Kinetics of PKCε activating and inhibiting llama single chain antibodies and their effect on PKCε translocation in HeLa cells, PLoS One 7 (2012), e35630, https://doi.org/10.1371/journal.pone.0035630.
[10] I. Van Audenhove, C. Boucherie, L. Pieters, O. Zwaenepoel, B. Vanloo, E. Martens, C. Verbrugge, G. Hassanzadeh-Ghassabeh, J. Vandekerckhove, M. Cornelissen, A. De Ganck, J. Gettemans, Stratifying fascin and cortactin function in invadopodium formation using inhibitory nanobodies and targeted subcellular delocalization, FASEB J. 28 (2014) 1805–1818, https://doi.org/10.1096/fj.13-242537.
[11] J. Bethuyne, S. De Gieter, O. Zwaenepoel, A. Garcia-Pino, K. Durinck, A. Verhelle, G. Hassanzadeh-Ghassabeh, F. Speleman, R. Loris, J. Gettemans, A nanobody modulates the p53 transcriptional program without perturbing its functional architecture, Nucl. Acids Res. 42 (2014) 12928–12938, https://doi.org/10.1093/nar/gku962.
[12] A. Steels, L. Vannevel, O. Zwaenepoel, J. Gettemans, Nb-induced stabilisation of p53 in HPV-infected cells, Sci.Rep. 9 (2019) 12680, https://doi.org/10.1038/s41598-019-49061-9.

[13] A. Steels, A. Verhelle, O. Zwaenepoel, J. Gettemans, Intracellular displacement of p53 using transactivation domain (p53 TAD) specific nanobodies, MAbs 10 (2018) 1045–1059, https://doi.org/10.1080/19420862.2018.1502025.
[14] G. Veggiani, G. Ossolengo, M. Aliprandi, U. Cavallaro, A. de Marco, Single-domain antibodies that compete with the natural ligand fibroblast growth factor block the internalization of the fibroblast growth factor receptor1, Biochem. Biophys. Res. Commun. 408 (2011) 692–696, https://doi.org/10.1016/j.bbrc.2011.04.090.
[15] A. Roy, A. Kucukural, Y. Zhang, I-TASSER: a unified platform for automated protein structure and function prediction, Nat. Prot. 5 (2010) 725–738, https://doi.org/10.1038/nprot.2010.5.
[16] A.B. Ward, P. Szewczyk, V. Grimard, C.W. Lee, L. Martinez, R. Doshi, A. Caya, M. Villaluz, E. Pardon, C. Cregger, D.J. Swartz, P.G. Falson, I.L. Urbatsch, C. Govaerts, J. Steyaert, G. Chang, Structures of P-glycoprotein reveal its conformational flexibility and an epitope on the nucleotide-binding domain, Proc. Natl. Acad. Sci. U. S. A. 110 (2013) 13386–13391, https://doi.org/10.1073/pnas.1309275110.
[17] Y.J. Park, T. Budiarto, M. Wu, E. Pardon, J. Steyaert, W.G.J. Hol, The structure of the C-terminal domain of the largest editosome interaction protein and its role in promoting RNA binding by RNA-editing ligase L2, Nucl. Acids Res. 40 (2012) 6966–6977, https://doi.org/10.1093/nar/gks369.
[18] N. Guex, M.C. Peitsch, SWISS-MODEL and the Swiss-Pdb Viewer: an environment for comparative protein modeling, Electrophoresis 18 (1997) 2714–2723, https://doi.org/10.1002/elps.1150181505.
[19] K. Lindorff-Larsen, S. Piana, K. Palmo, P. Maragakis, J.L. Klepeis, R.O. Dror, D. E. Shaw, Improved side-chain torsion potentials for the Amber ff99SB protein force field, Proteins 78 (2010) 1950–1958, https://doi.org/10.1002/prot.22711.
[20] G. Bussi, D. Donadio, M. Parrinello, Canonical sampling through velocity rescaling, J. Chem. Phys. 126 (2007), 014101, https://doi.org/10.1063/1.2408420.
[21] B. Hess, H. Bekker, H.J. Berendsen, J.G. Fraaije, LINCS: a linear constraint solver for molecular simulations, J. Comput. Chem. 18 (1997) 1463–1472, https://doi.org/10.1021/ct700200b.
[22] S. Pronk, S. Páll, R. Schulz, P. Larsson, P. Bjelkmar, R. Apostolov, M.R. Shirts, J. C. Smith, P.M. Kasson, D. van der Spoel, B. Hess, E. Lindahl, GROMACS 4.5: a high-throughput and highly parallel open source molecular simulation toolkit, Bioinformatics 29 (2013) 845–854, https://doi.org/10.1093/bioinformatics/btt055.
[23] F. Fogolari, A. Corazza, V. Yarra, A. Jalaru, P. Viglino, G. Esposito, Bluues: a program for the analysis of the electrostatic properties of proteins based on generalized Born radii, BMC Bioinformatics 13 (2012) S18, https://doi.org/10.1186/1471-2105-13-S4-S18.
[24] S.J. De Vries, M. van Dijk, A.M. Bonvin, The HADDOCK web server for data-driven biomolecular docking, Nat. Protoc. 5 (2010) 883–897, https://doi.org/10.1038/nprot.2010.32.
[25] S.J. de Vries, A.M.J.J. Bonvin, CPORT: a consensus interface predictor and its performance in prediction-driven docking with HADDOCK, PlosONE 6 (2011), e17695, https://doi.org/10.1371/journal.pone.0017695.
[26] A. Monegal, D. Ami, C. Martinelli, H. Huang, M. Aliprandi, P. Capasso, C. Francavilla, G. Ossolengo, A. de Marco, Immunological applications of single domain llama recombinant antibodies isolated from a naïve library, Prot. Eng. Des. Sel. 22 (2009) 273–280, https://doi.org/10.1093/protein/gzp002.
[27] S. Djender, A. Schneider, A. Beugnet, R. Crepin, K.E. Desrumeaux, C. Romani, S. Moutel, F. Perez, A. de Marco, Bacterial cytoplasm as an effective cell compartment for producing functional VHH-based affinity reagents and Camelidae IgG-like recombinant antibodies, Microb. Cell Factories 13 (2014) (2014) 140, https://doi.org/10.1186/s12934-014-0140-1.
[28] G. Veggiani, B. Giabbai, M.S. Semrau, B. Medagli, V. Riccio, G. Bajc, P. Storici, A. de Marco, Comparative analysis of fusion tags used to functionalize recombinant antibodies, Prot. Expr. Purif. 166 (2020), 105505, https://doi.org/10.1016/j.pep.2019.105505.
[29] O.G. Folorunsho, S.F. Oloketuyi, E. Mazzega, H. Budasheva, A. Beran, M. Cabrini, D. Korte, M. Franko, A. de Marco, Nanobody-dependent detection of Microcystis aeruginosa by ELISA and thermal lens spectrometry, Appl. Biochem. Biotechnol. 193 (2021) 2729–2741, https://doi.org/10.1007/s12010-021-03552-6.
[30] V. Damiano, P. Spessotto, G.T. Vanin, Perin, R. Maestro, M. Santarosa, The autophagy machinery contributes to E-cadherin turnover in breast cancer, Front. Cell Dev. Biol. 8 (2020) 545, https://doi.org/10.3389/fcell.2020.00545.
[31] T. Noguchi, S. Oishi, K. Honda, Y. Kondoh, T. Saito, T. Kubo, M. Kaneda, H. Ohno, H. Osada, N. Fujii, Affinity-based screening of MDM2/MDMX-p53 interaction inhibitors by chemical array: identification of novel peptidic inhibitors, Bioorg. Med. Chem. Lett. 23 (2013) 3802–3805, https://doi.org/10.1016/j.bmcl.2013.04.094.
[32] A.J. Levine, p53, the cellular gatekeeper for growth and division, Cell 88 (1997) 323–331, https://doi.org/10.1016/s0092-8674(00)81871-1.
[33] I. Castanon, S. Von Stetina, J. Kass, M.K. Baylies, Dimerization partners determine the activity of the Twist bHLH protein during Drosophila mesoderm development, Development 128 (2001) 3145–3159.
[34] P. Bialek, B. Kern, X. Yang, M. Schrock, D. Sosic, N. Hong, H. Wu, K. Yu, D. M. Ornitz, E.N. Olson, M.J. Justice, G. Karsenty, A TWIST code determines the onset of osteoblast differentiation, Dev. Cell 6 (2004) 423–435, https://doi.org/10.1016/s1534-5807(04)00058-9.
[35] S. Gu, T.G. Boyer, M.C. Naski, Basic helix–loop–helix transcription factor TWIST1 inhibits transactivator function of master chondrogenic regulator Sox9, J. Biol. Chem. 287 (2012) 21082–21092, https://doi.org/10.1074/jbc.M111.328567.
[36] S. Li, S.E. Kendall, R. Raices, J. Finlay, M. Covarrubias, Z. Liu, G. Lowe, Y.H. Lin, Y. H. Teh, V. Leigh, S. Dhillon, S. Flanagan, K.S. Aboody, C.A. Glackin, TWIST1 associates with NF-κB subunit RELA via carboxyl-terminal WR domain to promote cell autonomous invasion through IL8 production, BMC Biol. 10 (2012) 73, https://doi.org/10.1186/1741-7007-10-73.
[37] C.M. Roberts, S.A. Shahin, J. Loeza, T.H. Dellinger, J.C. Williams, C.A. Glackin, Disruption of TWIST1-RELA binding by mutation and competitive inhibition to validate the TWIST1 WR domain as a therapeutic target, BMC Cancer 17 (2017) 184, https://doi.org/10.1186/s12885-017-3169-9.
[38] R. Crépin, D. Gentien, A. Duché, A. Rapinat, C. Reyes, F. Némati, G. Massonnet, D. Decaudin, S. Djender, S. Moutel, K. Desrumeaux, N. Cassoux, S. Piperno-Neumann, S. Amigorena, F. Perez, S. Roman-Roman, A. de Marco, Nanobodies against surface biomarkers enable the analysis of tumor genetic heterogeneity in uveal melanoma patient derived xenografts, Pigment Cell Melanoma Res. 30 (2017) 317–327, https://doi.org/10.1111/pcmr.12577.
[39] R. Crepin, G. Veggiani, S. Djender, A. Beugnet, F. Planeix, C. Pichon, S. Moutel, S. Amigorena, F. Perez, N. Ghinea, A. de Marco, Whole-cell biopanning with a synthetic phage display library of nanobodies enabled the recovery of follicle-stimulating hormone receptor inhibitors, Biochem. Biophys. Res. Comm. 493 (2017) 1567–1572, https://doi.org/10.1016/j.bbrc.2017.10.036.
[40] D.B. Yap, J.K. Hsieh, S. Zhong, V. Heath, B. Gusterson, T. Crook, X. Lu, Ser392 phosphorylation regulates the oncogenic function of mutant p53, Cancer Res. 64 (2004) 4749–4754, https://doi.org/10.1158/0008-5472.CAN-1305-2.
[41] K.D. Sullivan, M.D. Galbraith, Z. Andrysik, J.M. Espinosa, Mechanisms of transcriptional regulation by p53, Cell DeathDiffer. 25 (2018) 133–143, https://doi.org/10.1038/cdd.2017.174.
[42] C. McMahon, A.S. Baier, R. Pascolutti, M. Wegrecki, S. Zheng, J.X. Ong, S. C. Erlandson, D. Hilger, S. Rasmussen, A.M. Ring, A. Manglik, A.C. Kruse, Yeast surface display platform for rapid discovery of conformationally selective nanobodies, Nat. Struct. Mol. Biol. 25 (2018) 289–296, https://doi.org/10.1038/s41594-018-0028-6.
[43] J.E. Shin, A.J. Riesselman, A.W. Kollasch, C. McMahon, E. Simon, C. Sander, A. Manglik, A.C. Kruse, D.S. Marks, Protein design and variant prediction using autoregressive generative models, Nat. Commun. 12 (2021) 2403, https://doi.org/10.1038/s41467-021-22732-w.
[44] C. Ackaert, N. Smiejkowska, C. Xavier, Y.G.J. Sterckx, S. Denies, B. Stijlemans, Y. Elkrim, N. Devoogdt, V. Caveliers, T. Lahoutte, S. Muyldermans, K. Breckpot, M. Keyaerts, Immunogenicity risk profile of nanobodies, Front. Immunol. 12 (2021), 632687, https://doi.org/10.3389/fimmu.2021.632687.
[45] I. Jovčevska, S. Muyldermans, The therapeutic potential of nanobodies, BioDrugs 34 (2020) 11–26, https://doi.org/10.1007/s40259-019-00392-z.
[46] F.P. Polack, S.J. Thomas, N. Kitchin, J. Absalon, A. Gurtman, S. Lockhart, J. L. Perez, G. Pérez Marc, E.D. Moreira, C. Zerbini, R. Bailey, K.A. Swanson, S. Roychoudhury, K. Koury, P. Li, W.V. Kalina, D. Cooper, R.W. Jr, L.L. Frenck, Ö. Hammitt, H. Türeci, A. Nell, S. Schaefer, D.B. Ünal, S. Tresnan, P.R. Mather, U. Dormitzer, K.U. Şahin, W.C.Gruber Jansen, C4591001 Clinical Trial Group, safety and efficacy of the BNT162b2 mRNA Covid-19 vaccine, N. Engl. J. Med. 383 (2020) 32603–32615, https://doi.org/10.1056/NEJMoa2034577.